A Study of Flow in Open Orthogonal and Trapezoidal Channels with Gabion Walls

D. KASITEROPOULOU
Department of Environmental Studies,
University of Thessaly, Larissa,
GREECE

Abstract: - The turbulent characteristics of the flow in open channels with gabion walls are studied numerically. Two trapezoidal and one orthogonal channel are used along with four different heights: 100mm, 150mm, 200mm, and 250mm of sand roughness in the gabion walls. Calculations of velocity, pressure, turbulence kinetic energy and eddy viscosity show clearly that the presence of the roughness affect considerably the fluid motion. As expected, the rough elements affect the mean velocity inside the channel and near the walls. Near the solid walls, the velocity profile is significantly affected and sharply lower velocities are observed very close to the walls.

Key-Words: - Open channel flow, Gabions, Computational Fluid Dynamics, Turbulent flow, orthogonal channel, trapezoidal channel, computer simulation.

Received: October 25, 2022. Revised: August 13, 2023. Accepted: September 24, 2023. Published: October 6, 2023.

1 Introduction

The type and the roughness of the solid walls can affect considerably the turbulent characteristics of the flow in open channels. Experimentally there is a lot of interest for aquatic flows in channels with vegetation and gabion walls. These studies present the influence of the wall construction on the velocity, pressure, turbulence kinetic energy, and eddy viscosity distribution near the bottom and up to the channel.

Gabions are used to reduce energy loss, stabilize the hydraulic jump, [1], [2], [3], [4], and increase discharge coefficients, [5], [6]. Many investigators used gabion walls in road construction as retaining structures in areas with hills, [7], and in open channels for protection against bed and bank erosion, [8], [9], [10].

Many studies are performed in open channels whose bed is covered with vegetation. The study, [11], investigated mass and momentum transfer across the Sediment-Water and found that there is a variation of the mean flow and turbulence across the SWI as a function of a dimensionless permeability. The flow in open channels with vegetated solid walls was also investigated, [12], [13], [14], and found that the velocity distribution depends on the vegetation height.

The last, compared the experimental results with the results of a CFX-based numerical model and found that there is a good agreement between the two of them. In all cases examined the vegetation height can reduce the velocity values near the walls. The higher vegetation leads to lower velocities.

The study, [15], investigated the vegetation geometry and the drag resistance as a function of the flow depth. In this theory, they added the turbulent kinetic energy equation for the layers model. The study, [16], studied the vegetation influence on velocity distribution by using a model that solves the momentum and continuity equations for each element and uses the k-ε model for the turbulence modeling. The study, [17], investigated flows in gabion channels and observed that the zero-place displacement parameter decreases with the increase in the area density of roughness elements.

In this work, we numerically investigate the flow in open channels with gabion walls. Velocity, pressure, turbulence kinetic energy, and eddy viscosity patterns are presented according to the roughness height and the flow rate in two trapezoidal and one orthogonal open channel.

2 Mathematical Model – Numerical Simulation

2.1 Mathematical Model

The mathematical model of the turbulent flow in this work consists of the Reynolds-Averaged Navier-Stokes (RANS) equations coupled with the k-ε turbulence model. Each primitive flow variable is decomposed into an averaged-in-time part and a fluctuation term. For example, the velocity vector at

a point in the flow field is given as the sum of the time-averaged velocity $\vec{\bar{U}}$ and a time-dependent velocity fluctuation $\vec{u}$, i.e., we write

$$\vec{U} = \vec{\bar{U}} + \vec{u} \quad (1)$$

The time-averaged velocity vector is defined as

$$\vec{\bar{U}} = \frac{1}{\Delta t}\int_{f}^{f+\Delta t} \vec{U} dt \quad (2)$$

where T is a time interval much longer than the characteristic periods of the turbulence fluctuations. The use of mean values (in time) in the conservation equations leads to the Reynolds-Averaged Navier-Stokes (RANS) equations:

$$\frac{\partial \rho}{\partial t} + \nabla \bullet \left(\rho \vec{U}\right) = 0 \quad (3)$$

$$\frac{\partial \rho \vec{U}}{\partial t} + \nabla \bullet \left(\rho \vec{U} \otimes \vec{U}\right) = \nabla \bullet \left(\tau - \rho \overline{\vec{u} \otimes \vec{u}}\right) + \vec{S}_M \quad (4)$$

In Equation (4), $\rho \overline{\vec{u} \otimes \vec{u}}$ are the Reynolds stresses and τ denotes the stress tensor due to molecular viscosity.

After introducing the concept of an effective viscosity, $\mu_{eff,}$ the conservation of mass equation is unchanged and the conservation of momentum equation is written as

$$\frac{\partial \rho \vec{U}}{\partial t} + \nabla \bullet \left(\rho \vec{U} \otimes \vec{U}\right) - \nabla \bullet \left(\mu_{eff} \nabla \vec{U}\right) = -\nabla p' + \nabla \bullet \left(\mu_{eff} \nabla \vec{U}\right)^T + \vec{B} \quad (5)$$

where $\vec{B}$ is the total body force per unit mass, μ_{eff} is the effective viscosity, and p′ is the modified pressure defined as

$$p' = p + \frac{2}{3}\rho k + \nabla \bullet \vec{U}\left(\frac{2}{3}\mu_{eff} - \zeta\right) \quad (6)$$

In Equation (6), ζ is the fluid bulk viscosity, ρ is the fluid density and k denotes the turbulent kinetic energy.

The k-ε model is used in this work for the calculation of the turbulent viscosity at each point of the flow field. The k-ε model is a two differential equation model where the effective viscosity is calculated as the sum of turbulent viscosity (μ_t) and molecular viscosity (μ) i.e.,

$$\mu_{eff} = \mu + \mu_t \quad (7)$$

The turbulent viscosity is computed at each point of the flow field in terms of the turbulence kinetic energy, k, and the turbulence kinetic energy dissipation rate, ε, by the relation

$$\mu_t = C_\mu \rho \frac{k^2}{\varepsilon} \quad (8)$$

where $C_\mu = 0{,}09$

The required values of k and ε are computed at each point of the turbulent flow field by concurrently solving the following two partial differential equations, [18]:

$$\frac{\partial(\rho k)}{\partial t} + \nabla \bullet (\rho \vec{U} k) = \nabla \bullet [(\mu + \frac{\mu_t}{\sigma_k})\nabla k] + P_k - \rho\varepsilon \quad (9)$$

$$\frac{\partial(\rho \varepsilon)}{\partial t} + \nabla \bullet (\rho \vec{U} \varepsilon) = \nabla \bullet [(\mu + \frac{\mu_t}{\sigma_\varepsilon})\nabla \varepsilon] + \frac{\varepsilon}{k}(C_{e1} P_k - C_{e2}\rho\varepsilon) \quad (10)$$

where $C_{e1} = 1{,}45$, $C_{e2} = 1{,}90$, $\sigma_k = 1{,}00$, $\sigma_\varepsilon = 1{,}30$ and P_k is the rate of production of turbulence kinetic energy calculated by

$$P_k = \mu_t \nabla \vec{U} \bullet (\nabla \vec{U} + \nabla \vec{U}^T) - \frac{2}{3}\nabla \bullet \vec{U}(3\mu_t \nabla \bullet \vec{U} + \rho k) \quad (11)$$

The ANSYS-CFX, [19], computer package is used in this work under the assumption of incompressible flow with constant properties (ρ= constant, μ= constant) and bulk viscosity ζ=0.

2.2 Channel Geometry and Modeling

We use a 3D model to study the flow inside: 1) case1: a trapezoidal channel of bottom width 2m, top width 6m and flow depth 1m, 2) case 2: a trapezoidal channel of bottom width 2m, top width 4m and flow depth 1m and 3) case3: an orthogonal channel of bottom width 3m and flow depth 1m. The gabion channel walls were simulated as gravel bed walls with four different gravel: 100mm, 150mm, 200mm, and 250mm. To minimize the computational burden we simulated flow by using periodic boundary conditions in the main flow direction. Consequently, our computational domain has a length of 1m. A 3-D (isometric) view of the computational domain is shown in Figure 1. Five values of discharge were used: Q_1=0.52m^3/s, Q_2=0.79 m^3/s, Q_3=1.58 m^3/s, Q_4=15.41 m^3/s, Q_5=41.96 m^3/s.

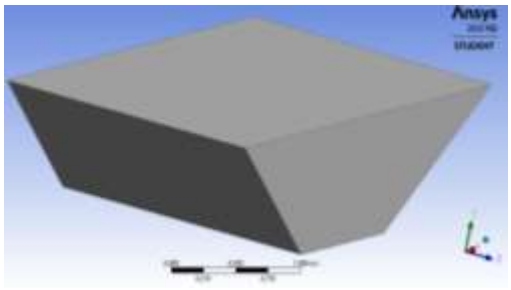

Fig. 1: A 3-D view of the channel as modeled in the ANSYS-CFX environment

2.3 Boundary Conditions and Mesh Design

To complete the mathematical model, the free slip boundary condition was specified at the free surface. In solid weir flows walls were assumed smooth without slip velocity (no-slip boundary condition) whereas at the gabion channels, four different gravel diameters were used to simulate sand-grained roughness. A 3-D view of the mesh generated using the ANSYS-CFX preprocessor is shown in Figure 2.

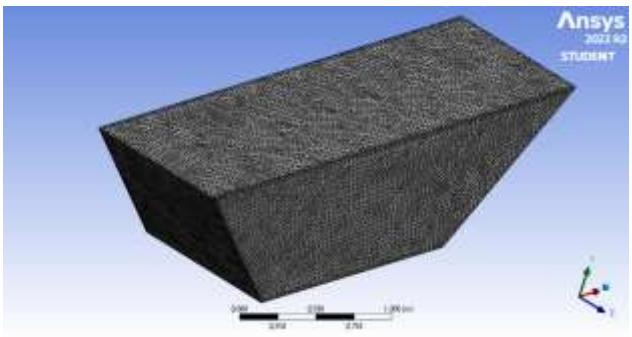

Fig. 2: A 3-D view of the mesh. Case 2

The computational domain has been discretized using tetrahedral elements. Three to six mesh designs were evaluated to choose the optimal/suboptimal mesh and ensure that the solution is independent of the mesh used. Sensitivity to global quantities, such as mass conservation helped judge the approximate convergence of the solutions. The mesh finally chosen provides a good balance between the stability of the solution and the flow field resolution. The grid for the three mesh designs used for all cases is shown in Table 1.

Table 1. Mesh Parameters

Case 1: Trapezoidal channel of bottom width 2m, top width 6m and flow depth 1m			
Number of nodes	Number of tetrahedra	Mean velocity (m/s)	% difference
24576	129705	0.132513	1,875%
28595	143924	0.130028	3,556%
28843	153355	0.125404	5,364%
Case 2: Trapezoidal channel of bottom width 2m, top width 4m and flow depth 1m			
Number of nodes	Number of tetrahedra	Mean velocity (m/s)	% difference
16894	61775	0.150953	5.88%
17481	63918	0.142566	4.799%
18409	67400	0.149753	0.795%
Case 3: Orthogonal channel of bottom width 3m and flow depth 1m			
Number of nodes	Number of tetrahedra	Mean velocity (m/s)	% difference
15855	58015	0.13723	3.204%
16282	59748	0.13297	1,824%
16672	61099	0.135442	1,303%

3 Results and Discussion

Various aspects of the computed 3-D velocity field are presented in Figure 3, Figure 4, Figure 5, and Figure 6. The calculated dimensionless mean total velocity for constant discharge is shown in Figure 3 and Figure 4 for the coarse grid (Mesh 3). The dimensionless velocity is useful when comparing the computational results obtained with channel flows of different gravel bed roughness diameters and different geometries.

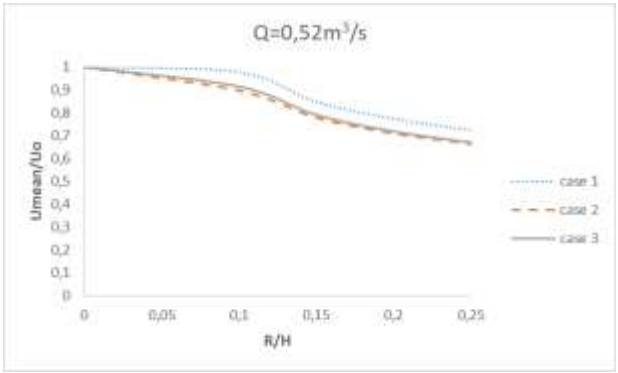

Fig. 3: Computed mean dimensional total velocity value. Q=0,52m^3/s

We observe that the total velocity value depends on the roughness size, the geometry shape, and the

flow rate. In particular, for constant discharge equal to Q=0,52m3/s as the gravel diameter increases for the same geometry channel shape the mean velocity decreases. Moreover, for the same gravel diameter, we observe that case 1 reveals larger values than cases 2 and 3 where values are close enough. Regarding now larger discharge (Figure 4) we observe that as the gravel diameter increases the dimensional velocity decreases but the values for all channel shapes are close enough.

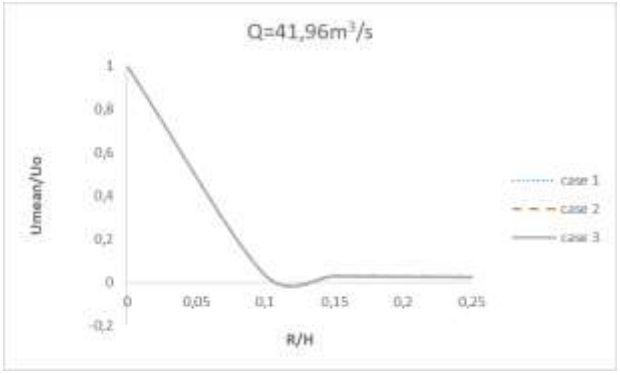

Fig. 4: Computed mean dimensional total velocity value. Q=41,96m^3/s

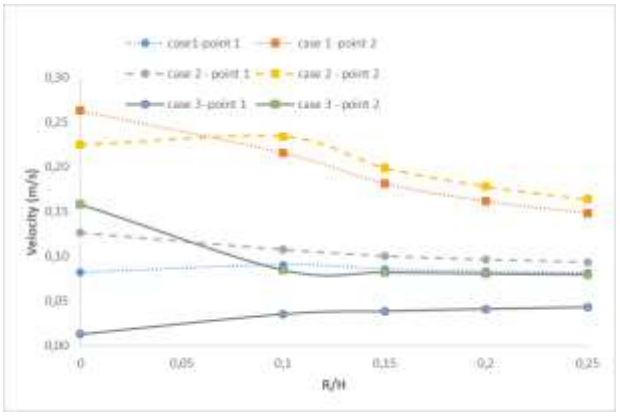

Fig. 5: Streamwise velocity value near the bottom (point 1: 3, 0.05, 0.5) and near the top of the channel (point 2: 3, 0.95, 0.5). Volume flow rate Q = 0.79 m^3/s.

The streamwise velocity for constant discharge near the bottom and the top of the channel is presented in Figure 5. The velocity at these points is useful to investigate how the gravel bed can affect the flow pattern. Again, we observe that the gravel effect is important both near the bottom and near the top of the channel. However, when comparing smooth and rough solid walls, we note that the velocity values are significantly affected by the roughness because sharply lower velocities are observed very close to the rough walls: for example, in case 2 the velocity near the smooth wall is 0.13m/s while near the rough walls is 0.08m/s (the last can also be observed in Figure 6).

We also observe that the channel shape along with the gravel diameter can affect considerably the velocity values at the top of the channel. Velocity values near the top of the channel in case 2 is higher than in case 1 and 3. In all cases, the gravel effect is important, and sharply lower values are detected when the gravel diameter increases.

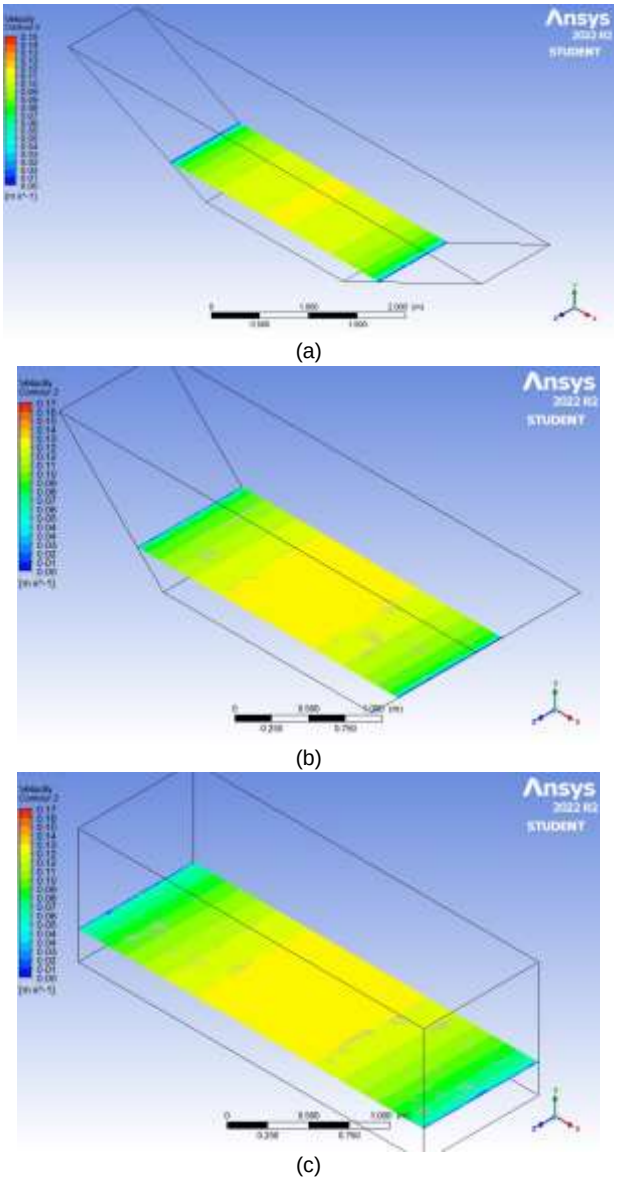

Fig. 6: Contour plots of speed velocity at depth y = 0.250 m, for the channel with gravel 250mm (R250). (a) case1, (b) case2, (c) case3. Volume flow rate Q = 0.79 m^3/s.

At the bottom of the channel, a nearly linear velocity profile is exhibited in the turbulent case and is completely dominated by viscous effects. It should be noted that to accurately resolve the

boundary layers, an extremely fine grid must be used and, even if the resolution is adequate, the mean (in time) turbulent velocity profile is not modeled adequately when wall functions are used in the implementation of the k-ε model. For a discussion on k-ε model modification, to resolve the boundary layer up to the solid wall, [18].

Regarding the computed total mean dimensional pressure along the channel presented in Figure 7, Figure 8 and Figure 9 we observe that as the volume flow rate increases the effect of the gravel diameter becomes more important. For the same volume flow rate the total mean pressure decreases as the grain diameter increases whereas, for the same roughness the total pressure increases as the volume flow rate also increases. It is important to notice that in case 1 the reduction is lower than in case 2 and 3 when the gravel diameter increases. Cases 2 and 3 reveal lower velocities than in case 1 for the same discharge and the same gravel diameter, meaning that gravel effects are more important in bigger shapes for low discharges.

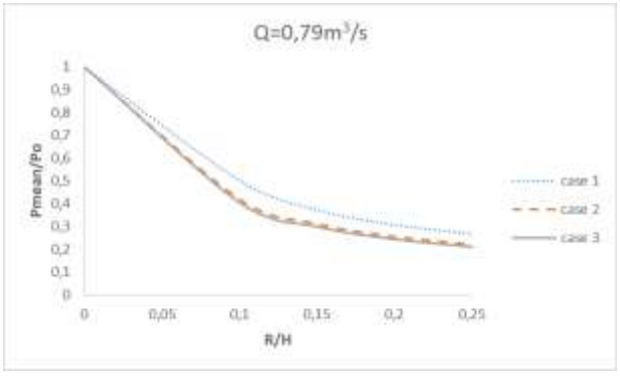

Fig. 7: Computed mean dimensional total pressure value. Q=0,79m^3/s

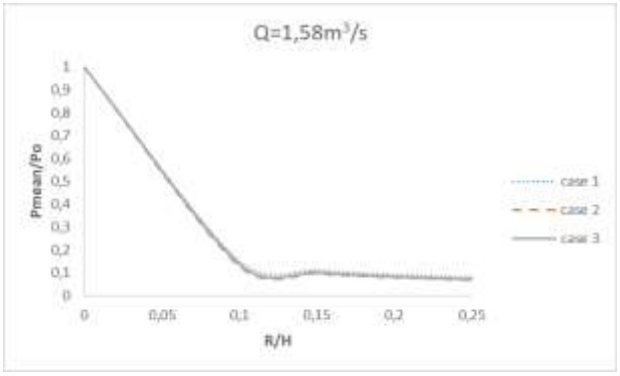

Fig. 8: Computed mean dimensional total pressure value. Q=1,58m^3/s

Examining the distribution of the turbulence kinetic energy (Figure 9) and the turbulence kinetic energy value near the bottom (point 3, 0.05, 0.5) and near the top of the channel (point 3, 0.95, 0.5) (Figure 10) we observe that lower values are detected as we move closer to the top of the channel for smooth and rough channels. Near the bottom of the channel higher values are detected in the rough channels for all channel shapes and the thickness of the maximum turbulence kinetic energy layer depends on the roughness height and the shape of the channel.

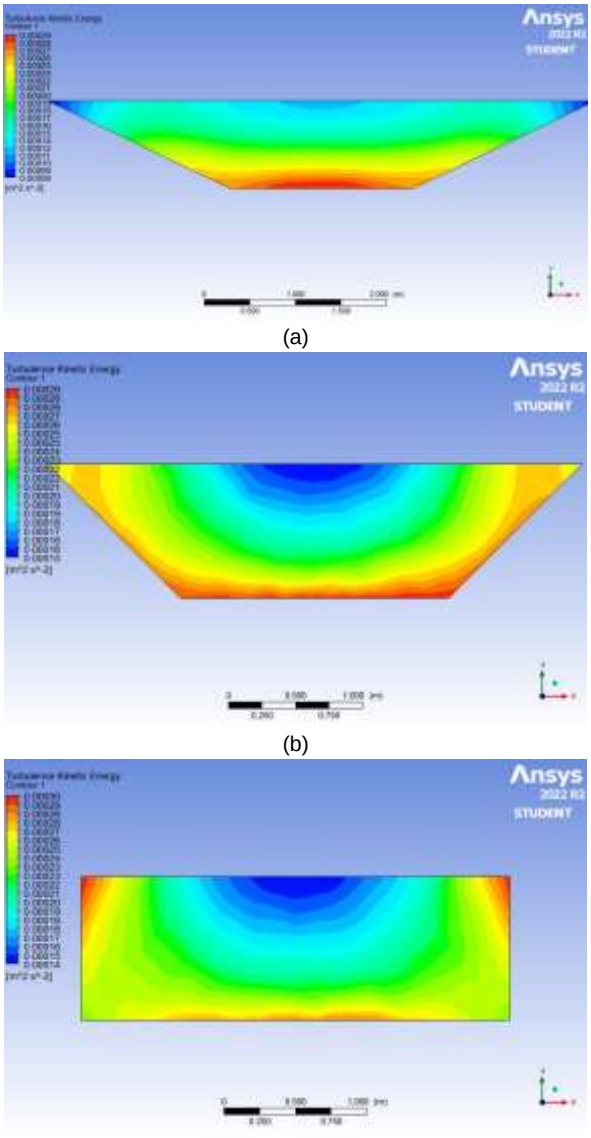

(a)

(b)

(c)

Fig. 9: Turbulence Kinetic energy distribution on midplane z=0.5 m for the channel with gravel 250mm (R250). (a) case1, (b) case2, (c) case3. Volume flow rate Q = 0.79 m^3/s.

We also observe that in case 1 as the roughness increases the turbulence kinetic energy decreases near the bottom whereas in cases 2 and 3 higher velocity values are detected at the bottom of the channel as the gravel diameter increases. According

to the top of the channel, we observe that the turbulence kinetic energy increases as the roughness height increases for all channel shapes.

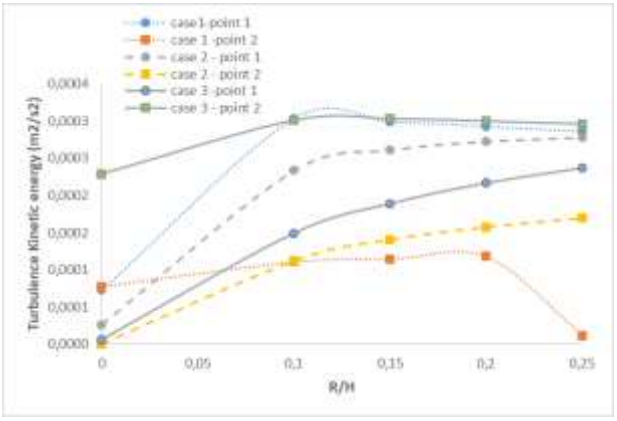

Fig. 10: Turbulence Kinetic energy value near the bottom (point 1: 3, 0.05, 0.5) and near the top of the channel (point 2: 3, 0.95, 0.5). Volume flow rate Q = 0.79 m^3/s.

In Figure 11, the eddy viscosity distribution for the channel with gabions of gravel diameter 250mm is presented for all channel shapes. We observe that low eddy viscosity values are detected at the solid side walls near the surface for all cases and high eddy viscosity values are observed in the central part of the channel throughout the depth of the channel. In Figure 10, we observe that both near the surface and the bottom of the channel the eddy viscosity increases as the roughness increases for constant flow rate. Therefore, it is concluded, that the gabion roughness increases eddy viscosity values in a much greater volume of the channel for both orthogonal and trapezoidal channels.

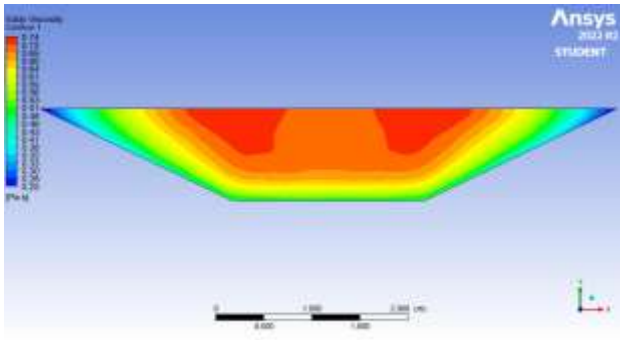

(a)

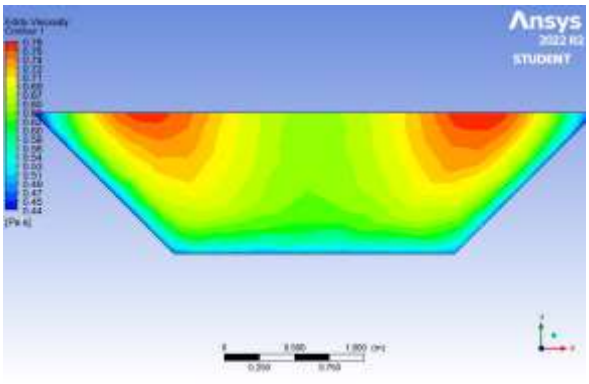

(b)

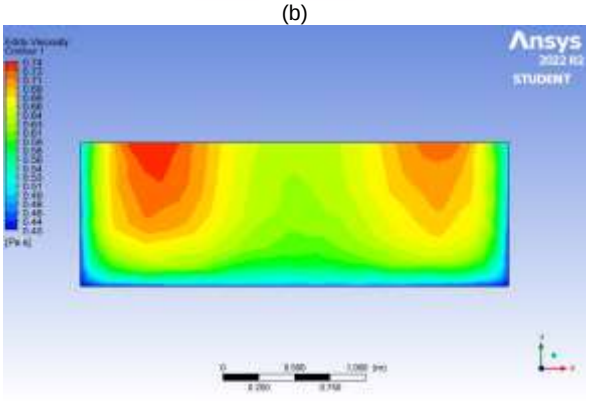

(c)

Fig. 11: Eddy viscosity distribution on midplane z=0.5 m for the channel with gravel 250mm (R250). (a) case1, (b) case2, (c) case3. Volume flow rate Q = 0.79 m^3/s.

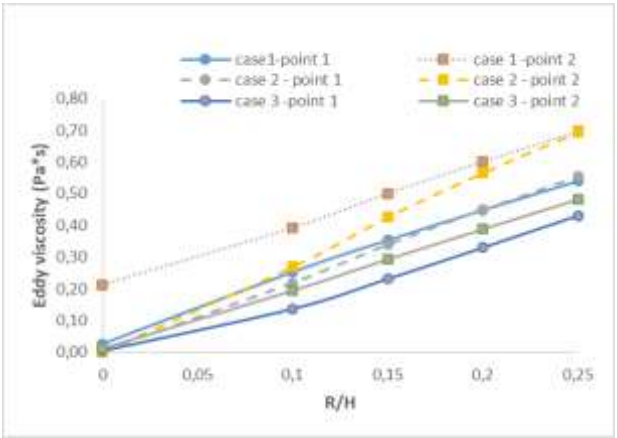

Fig. 12: Eddy viscosity value near the bottom (point 1: 3, 0.05, 0.5) and near the top of the channel (point 2: 3, 0.95, 0.5). Volume flow rate Q = 0.79 m^3/s.

4 Conclusion

In this paper, we have presented the simulations of turbulent flow in two trapezoidal and one orthogonal channel whose walls are simulated as gabion walls. The gabion walls are modeled by sand roughness of four different heights: 100mm, 150mm, 200mm, and 250mm. Calculations of velocity, pressure, turbulence kinetic energy, and eddy viscosity (Figure 12) show clearly that the presence of the roughness affects considerably the fluid motion for all channel shapes examined. As expected, the rough elements affect the mean velocity inside the channel and near the walls and this effect becomes more important depending on the channel shape. Near the solid walls, the velocity profile is significantly affected and sharply lower velocities are observed very close to the walls. The last behavior becomes more important for bigger channel shapes at low discharges.

For the same volume flow rate the total mean pressure decreases as the grain diameter increases. Moreover, at the top of the channel, the turbulence kinetic energy and the eddy viscosity increase as the roughness increases for a constant flow rate for all channel shapes.

References:

[1] M.R. Simac, R.J. Bathurst and T.W. Fennessey, Design of Gabion - Geosynthetic Retaining Walls On the Tellico Plains to Robbinsville Highway, *Geosynthetics '97 Conference*, California, USA, pp. 105-118, March 1997.

[2] I. Nešović, S. Paunović, M. Petrović and N. Ćirić, The Stability of Gravity Retaining Structures, *41th Anniversary Faculty of Civil Engineering Subotica, International Conference Contemporary achievements in civil engineering*, 24 April 2015, Subotica, SERBIA.

[3] K. K. Gupta and S. Kumar, Flow Characteristics of Gabion Weir for Free Flow Condition – an Experimental Approach, *International Journal of Advanced Research in Engineering and Technology (IJARET)*, vol.11, no. 8, pp. 889-898, August 2020, doi: 10.34218/IJARET.11.8.2020.087.

[4] R. Daneshfaraz, M. Bagherzadeh, A. Ghaderi, S. Francesco and M. Asl, Experimental Investigation of Gabion Inclined Drops as a Sustainable Solution for Hydraulic Energy Loss, Ain Shams Engineering Journal, vol. 12, no. 4, pp. 3451-3459, December 2021, doi: https://doi.org/10.1016/j.asej.2021.03.013.

[5] D. Kasiteropoulou, G. Papapolymerou, X. Spiliotis and D. Christodoulou, Numerical study of turbulent flow in gabion open channels, *International Journal of Research in Engineering and Science*, vol.10, no.5, pp.1-8, 12 May 2022.

[6] R. Biabani, F. Salmasi, M. Nouri and J. Abraham, Flow Over Embankment Gabion Weirs in Free Flow Conditions, *Research Square*, preprint, 01 Jun 2021, doi: https://doi.org/10.21203/rs.3.rs-572510/v1.

[7] N. Utmani, S. Ahmad, R.U.I. Islam and M. Abbas, Gabion Wall used in Road Construction and Flood Protection Embankment, *Journal of Civil Engineering and Environmental Sciences*, vol. 5, no. 1, pp. 001-004, January 2019, doi: 10.17352/2455-488X.000031.

[8] Y.T.A. Khalid, and M.A.N. Bahzad, Protection of Open Channels Using Gabions, *AL – Rafdain Enginnering Journal*, vol. 18, no. 2, pp. 36-48, April 2010, doi: 10.33899/rengj.2010.28176.

[9] M. Pallavi and L. Harshith, Open Channel Flow Characteristics using Gabion Weir, *International Research Journal of Engineering and Technology*, vol. 05, no.12, pp.928-933, December 2018.

[10] T. Craswell and S. Akib, Reducing Bridge Pier Scour Using Gabion Mattresses Filled with Recycled and Alternative Materials, *Eng*, vol. 1, no. 2, pp. 188–210, 31 October 2020, doi:10.3390/eng1020013.

[11] J.J. Voermans, M. Ghisalberti and G.N. Ivey, The variation of flow and turbulence across the sediment-water interface, *Journal of Fluid Mechanics*, vol. 824, pp. 413–437, 06 July 2017, doi: https://doi.org/10.1017/jfm.2017.345.

[12] D. Kasiteropoulou, A. Liakopoulos, N. Michalolias and E. Keramaris, Numerical Modelling and Analysis of Turbulent Flow in an Open Channel with Submerged Vegetation, *Environmental Processes* vol. 4, pp. 47–61, 09 May 2017, doi: https://doi.org/10.1007/s40710-017-0235-x.

[13] E. Keramaris, D. Kasiteropoulou, A. Liakopoulos, N. Michalolias and G. Pechlivanidis, A study of flow in open channels with vegetation: Experiments and numerical models, *Special Topics & Reviews in Porous Media*, vol. 8, pp. 109–129, January 2017, doi: 10.1615/SpecialTopicsRevPorousMedia.2017019692.

[14] N. Michalolias, E. Keramaris, D. Kasiteropoulou, A. Liakopoulos and G. Pechlivanidis, Experiments and Numerical Analysis of Flow in an Open Channel with Gravel Bed, *Proceedings*, vol. 2, pp. 581-590, 30 July 2018, doi:10.3390/proceedings2110581, pp. 1-9.

[15] A. Defina and A.C. Bixio, Mean flow and turbulence in vegetated open channel flow, *Water Resources Research*, vol. 41, no.7, 08 July 2005, doi: 10.1029/2004WR003475.

[16] C.A.M.E. Wilson, O. Yagci, H.P. Rauch and N.R.B. Olsen, 3D numerical modeling of a willow vegetated river/floodplain system, *Journal of Hydrology*, vol. 327,no. 1-2, pp. 13–21, 30 July 2006, doi: https://doi.org/10.1016/j.jhydrol.2005.11.027.

[17] C.W. Li and J. Li, DANS model for vegetated open channel flows, *Journal of Hydraulic Research*, vol. 53, no. 6, pp. 699-713, 12 September 2015, doi: https://doi.org/10.1080/00221686.2015.1054320.

[18] A. Liakopoulos, Fluid mechanics. *Tziolas Publications*, 2010 (in greek).

[19] ANSYS-CFX, Release 11.0 – User Guide.

Contribution of Individual Authors to the Creation of a Scientific Article (Ghostwriting Policy)

The authors equally contributed in the present research, at all stages from the formulation of the problem to the final findings and solution.

Sources of Funding for Research Presented in a Scientific Article or Scientific Article Itself

No funding was received for conducting this study.

Conflict of Interest

The authors have no conflict of interest to declare.